*29th EPS Conference on Plasma Phys. and Contr. Fusion Montreux, 17-21 June 2002 ECA Vol. **26B**, P-4.073 (2002)*

Modeling of Enhanced Scattering in Dense Plasmas

E.Z.Gusakov[1], M.A.Irzak[1], M.Krämer[2], V.L.Selenin[1].

[1] *A.F.Ioffe Physico-Technical Institute, 194021 St Petersburg, Russia.*
[2] *Institut für Experimentalphysik II, NB5, D-44780 Bochum, Germany.*

1. Introduction

The enhanced scattering (ES) technique has been successfully applied for studying plasma density fluctuations near the upper hybrid resonance (UHR) of the probing wave both in linear plasma devices and in tokamaks [1]. The key issue in this diagnostics is the accessibility of the UHR. In standard tokamak experiments the probing was performed from the high magnetic field side of the torus from where the UHR is accessible. In a majority of linear devices the probing waves possessing wavelength larger than the plasma size was used thus guaranteeing sufficient power penetration to the UHR.

In the present paper we show by numerical modeling that new areas of application of ES technique exist in high density plasma of helicon discharges or spherical tokamaks immersed in a low magnetic field for which inequality $\omega_{pe} >> \omega_{ce}$ usually holds. The distance between the cutoff and the UHR is then very small even in large devices so that the probing wave can easily penetrate the cut-off layer.

2. Model and computational results

We employed a model that takes into account the realistic geometry of plasma and antenna. The task is divided into three parts: (1) modeling of the antenna (determining the actual 2D diagram and the received signal); (2) modeling of the wave propagation inside the plasma volume (solving a 1D full electro-magnetic plasma wave equation); (3) modeling of the enhanced scattering process in the vicinity of the upper hybrid resonance layer. The developed model was mainly applied to interpret the ES measurements carried out on the helicon device HE-L (plasma radius $a = 7$ cm, $B_0 = 30$–80 mT, radial density profile $n_e = n_{e0}\cdot\exp(-(r/w_0)^2)$ with $n_{e0} \approx 10^{13}$ cm^{-3} and $w_0 = 3$ cm, $T_e \approx 3$ eV, main ion species Ar^+ [2])

(1) Antenna modeling. The rectangular horn antenna was modeled in the "long horn" approximation (justified by the real horn dimensions), that is, the horn was replaced by a rectangular waveguide having the same cross-section as the horn aperture. The electromagnetic field inside the waveguide is represented by a series of eigenmodes of sufficiently large number and given amplitudes of the incident modes. After determining the plasma surface impedance (see next section) we match the fields at the waveguide opening and at the plasma surface to obtain a self-consistent set of algebraic equations for the unknown amplitudes of the reflected waveguide modes. The solution allows us to reconstruct the actual electric field in the waveguide and determine the signal backscattered from the plasma.

(2) Wave propagation modeling. To model the wave propagation inside the plasma column a full electro-magnetic cold plasma wave equation is solved in the 1D cylindrical geometry. All plasma parameters are assumed to vary only in radial (r) direction, so the wave field is Fourier decomposed in the azimuthal (θ) and axial (z) directions. To model absorption in the UHR we introduce the complex wave frequency $\omega = \omega_0 + i\nu$ (where ν is an effective

collision frequency).

(3) Enhanced scattering modeling. To model the enhanced scattering process in the vicinity of the UHR layer we used two different approaches. Both of them make use of the fact that the RF energy of the incident wave coupled to the Bernstein wave is exactly equal to that absorbed near the UHR in cold plasma approximation. Thus, we obtain the correct information on the coupling efficiency from our cold plasma model.

The first approach is based purely on the numerical calculations and solves the plasma wave equation throughout the whole plasma volume including the UHR region in the presence of density fluctuations. The latter were introduced as a sine-like static perturbation of the radial density profile. The second, analytical approach is based on the reciprocity theorem and allows one to determine the scattered signal from a given level of the density fluctuations. It requires information on the linear conversion coefficient obtained again from the numerical computation, but with a smooth density profile [1].

Using the first approach we had to assume an ideally conducting wall surrounding the plasma column (which is not adequate to the experimental conditions). As the single-pass RF power absorption in the plasma is small, we get a resonator with a high Q factor. To overcome this we introduced a cylindrical absorbing layer ($\varepsilon = 1 + i\kappa$) between the metal wall and plasma surface. The width of the layer and value of κ were chosen to provide the necessary reduction of the Q factor (75% single pass power absorption in the layer at 9 GHz).

The dependence of the scattered signal on the amplitude of the density fluctuations is presented in Fig. 1 ($f = 9$ GHz, $n_{e0} = 10^{13}\text{cm}^{-3}$, $B = 60$ mT, $\nu/\omega_0 = 2\cdot10^{-4}$, $\delta n/n_{\text{UHR}} = 0.5\%$, $\lambda_{\text{fluct}} = 2$ mm, waveguide cross-section 5.6×3.4 cm^2). The two curves correspond to the cases when the density fluctuation has either a maximum or the minimum at the UHR surface. For $\delta n/n < 1\%$ the dependence is linear and the signal is independent of the phase of the fluctuations. At higher fluctuation level a non-linear dependence is observed.

Fig. 2 shows the dependence of the scattered signal on the central electron density for two different waveguide cross-sections. The signal variation is not large (by a factor of 2) in the range $n_{e0} = (1.2\text{–}30)\cdot10^{12}\,\text{cm}^{-3}$, but it falls down abruptly as the central density goes below $1.2\cdot10^{12}\,\text{cm}^{-3}$. At $n_{e0} = 1.2\cdot10^{12}\text{cm}^{-3}$ the UHR is located at $r = 1.4$ cm which is comparable with the antenna cross-section.

In the analytical approach we used the formula for enhanced scattering derived in [1]:

$$A_s = \frac{i\omega_i A_i}{16\pi n_e}\int E^+_{ar}(\vec{r})\delta n_\Omega(\vec{r})E_{ir}(\vec{r})d\vec{r}\,, \qquad (1)$$

$$\delta n_\Omega(\vec{r}) = \iint\frac{dq_z}{2\pi}\frac{dq_r}{2\pi}\frac{1}{2\pi r_{UHR}}\sum_{m_s=-\infty}^{+\infty}e^{-iq_z z - iq_r r - im_s\theta}\delta n_\Omega(q_r, m_s/r_{UHR}, q_z)\,, \qquad (2)$$

where E_{ir} and E_{ar}^+ are the wave fields at the UHR produced by the unity RF power from the emitting and receiving antennas, respectively (E_{ar}^+ is computed at a reversed direction of the static magnetic field); A_i and A_s are the wave amplitudes in the emitting and receiving antennas; q_z, q_r and m_s are the axial and radial wave numbers and an azimuthal mode number of the fluctuation, respectively. Backscattered power relates to the fluctuations amplitude as:

$$\frac{P_s(\Omega)}{P_i} = \int \frac{dq_z}{2\pi} \sum_{m_s=-\infty}^{+\infty} F(q_z, m_s) \int \frac{dq_r}{2\pi} (q_r l)^2 e^{-4\varepsilon^{im} q_r l} \frac{|\delta n|^2_{q_r, m_s/r_{UHR}, q_z}}{n_{UHR}^2}, \quad (3)$$

$$\text{where } F(q_z, m_s) = \frac{1}{2\pi r_{UHR}} \left| \int \frac{dk_z}{2\pi} \sum_{m=-\infty}^{+\infty} C_{k_z,m} \cdot C^{+}{}_{q_z - k_z, m_s - m} \cdot e^{im\Delta\theta_a} \right|^2, \quad (4)$$

$l = (\mathrm{d}\varepsilon^{re}/\mathrm{d}r)^{-1}$ is the characteristic length scale, $\Delta\theta_a$ is the azimuthal angle between the emitting and receiving antennas and $C_{k_z,m}$ is proportional to the wave electric field in UHR ($|C_{k_z,m}|^2$ is equal to the partial power absorbed in UHR for a unity incident power). An example of $C_{k_z,m}$ distribution for the same parameters as in previous figures is given in Fig. 3. One can see a significant asymmetry in respect to the azimuthal wave numbers. This is due to the effect of plasma gyrotropy which is well known in ion cyclotron and intermediate frequency range, but it appears to play an important role even at such high frequencies.

3 Experiment interpretation

Application of correlative ES to wave propagation study in HE-L device resulted in discovery of intensive scattering spectra in the range $0 < f_i - f_s < 5$ MHz [3]. The low frequency oscillations were proved to be of ion acoustic origin. The scattering spectrum has a maximum at $f_i - f_s = 1.5$ MHz and exhibits a fast decrease at larger frequency shifts. The estimation of measured scattering power resulted in power conversion coefficient $P_s(\Omega)\Delta\Omega/P_i = 3\cdot10^{-5}$. This data allows us to estimate the perturbation level for a given wave number spectrum.

In the case of isotropic and wide spectrum similar to that derived in [4] for kinetic ion acoustic instability $\left\langle \tilde{n}^2_{\vec{k}\omega} \right\rangle = \frac{16\pi^2 \delta n^2 \ln(1/kr_d)}{k^3 \ln(a/r_d)}$ we come to the expression for the ES signal:

$$\frac{P_s(\Omega)}{P_i} = 8\pi l^2 S \frac{1}{\Omega} \frac{\ln(\Omega_{pi}/\Omega)}{\ln^2(a/r_d)} e^{-4\varepsilon^{im} \frac{l\Omega}{v_s}} \left(\frac{\delta n}{n_{UHR}} \right)^2, \quad (5)$$

where $S = \int \frac{dq_z}{2\pi} \sum_{m_s=-\infty}^{+\infty} F(q_z, m_s)$ is shown in Fig. 4 as a function of angle $\Delta\theta_a$ for different probing frequencies. For the experimental value of $\Delta\theta_a = -27°$ we get $S = 3\cdot10^{-3}$ and come to the estimation of the density perturbation in the ion acoustic turbulence $\delta n/n_{\mathrm{UHR}} \approx 0.25$. This estimation is far too high for using the linear scattering model [1]. At such turbulence level the correlation analysis is complicated as multi-scattering occurs in the UHR region [5] leading to the probing wave extinction.

In the case of anisotropic spectrum with fluctuations running in radial direction we can use the results of full-wave computations shown in Fig. 1. Starting with the power conversion value of $3\cdot10^{-5}$, we readily get $\delta n/n_{\mathrm{UHR}} = 7\cdot10^{-3}$. At this value the scattered wave amplitude dependence on the perturbation level is still linear. If the perturbation amplitude is 3 times higher, nonlinear distortions play a significant role leading to the probing wave depletion. Taking into account that the actual fluctuation spectrum has some intermediate form between two limiting cases analyzed above we should conclude that the acoustic density perturbation satisfies an inequality $10^{-2} < \delta n/n_{\mathrm{UHR}} < 0.25$. If $\delta n/n_{\mathrm{UHR}} > 2\cdot10^{-2}$ the probing wave extinction

due to the scattering off this turbulence becomes important. This effect can explain quick scattering spectrum decay at higher acoustic wave frequencies.

Acknowledgements

This work was supported by the *Deutsche Forschungsgemeinschaft* through the Project KR 1058 and the *Russian-German Cooperation*, Contract 146 RUS 590.

References

[1] K. M. Novik and A. D. Piliya, Plasma Phys. Control. Fusion **35** (1993) 357.

[2] M. Krämer, Th. Enk and B. Lorenz, Physica Scripta **T84** (2000) 132.

[3] V. L. Selenin, M. Krämer, N. M. Kaganskaya, B. Lorenz, this conference, poster P-2.024.

[4] B. B. Kadomtsev, *Plasma turbulence*, Academic Press, N.Y., 1965

[5] E. Z. Gusakov, A. V. Surkov, this conference, poster P-2.127.

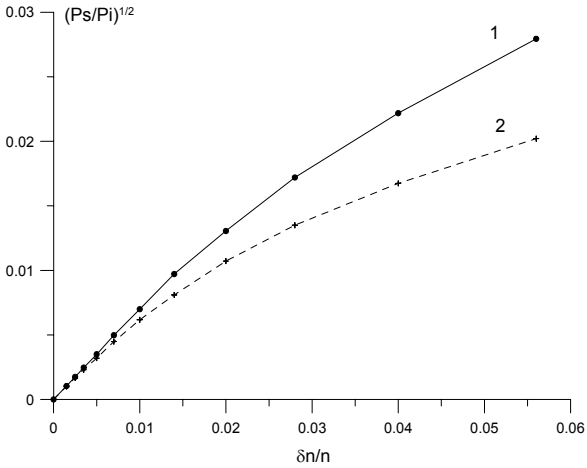

Fig. 1. Scattering signal versus oscillations amplitude. $n_{e0} = 10^{13} cm^{-3}$, $f = 9$ GHz, $B_0 = 60$ mT, $\lambda_{fluc} t = 2$ mm, horn 5.6×3.4 cm^2. Curve 1 — $\delta n/n > 0$, 2 — $\delta n/n < 0$ at the UHR.

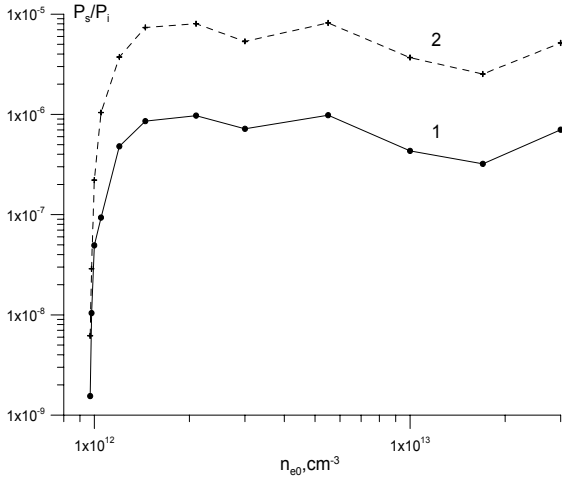

Fig. 2. Dependence of the scattering signal on the central density. $\delta n/n = 0.5\%$, other parameters are the same. Curve 1 — horn 2.3×1.0 cm^2, 2 — horn 4.0×2.2 cm^2

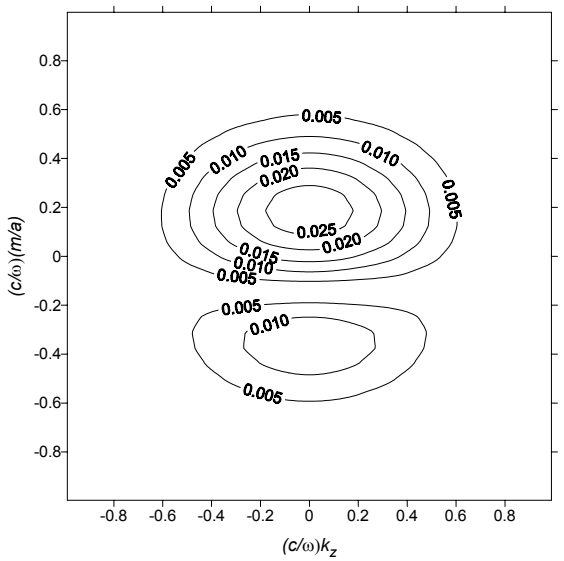

Fig. 3. Topological map of $|C|$ distribution for the horn 5.6×3.4 cm^2. Other parameters are the same.

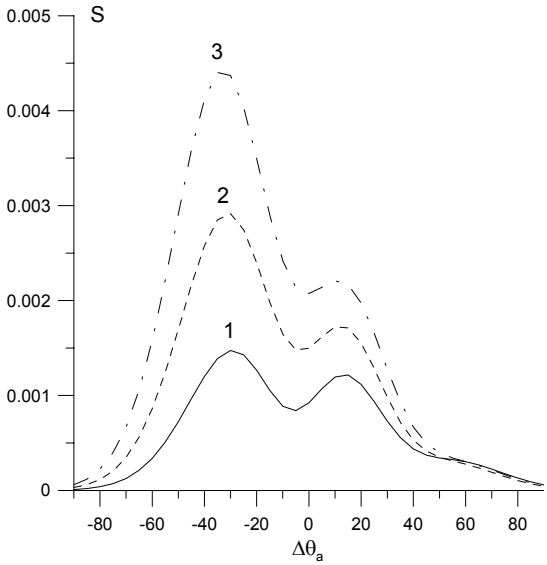

Fig. 4. Coefficient S versus $\Delta\theta_a$ for the same parameters. 1 — $f = 5$ GHz, 2 — $f = 9$ GHz, 3 — $f = 14$ GHz